Volume changes in a filled elastomer studied via digital image correlation

Jordan de Crevoisier[a,b], Gilles Besnard[a], Yannick Merckel[c], Huan Zhang[b], Fabien Vion-Loisel[d], Julien Caillard[d], Daniel Berghezan[d], Costantino Creton[b], Julie Diani[e], Mathias Brieu[c], François Hild[a], Stéphane Roux[a1]

[a] *LMT-Cachan (ENS de Cachan/CNRS/UPMC/PRES UniverSud Paris)*
61 avenue du Président Wilson, F-94235 Cachan, France
[b] *Physico-chimie des Polymères et des Milieux Dispersés, UMR7615,*
ESPCI/CNRS/UPMC, 10 rue Vauquelin, F-75005 Paris, France
[c] *LML, Ecole Centrale de Lille,*
bd Paul Langevin, F-59650 Villeneuve d'Ascq, France
[d] *Michelin, CERL Ladoux,*
F-63040 Clermont Ferrand, France
[e] *Laboratoire PIMM, CNRS, Arts et Métiers ParisTech,*
151 bd de l'Hôpital, F-75013 Paris, France

Abstract

Volumetric strains in a filled SBR specimen subjected to cyclic uniaxial tension with increasing extensions are studied. Digital image correlation is used to follow the kinematics of two orthogonal free faces. A volume expansion is observed past a critical elongation, which can be interpreted as the onset of cavitation. Under unloading, the volume returns to its original value and remains constant upon reloading. Increasing the elongation to higher values than the previous cycle leads again to a volumetric expansion.

Keywords: Elastomer, compressibility, cavitation, DIC, damage

---

[1] Corresponding author (stephane.roux@lmt.ens-cachan.fr)

1. Introduction

Incompressibility is a widely used assumption for the mechanical behaviour of filled and unfilled rubbers in most tests and models. This assumption is supported by the bulk modulus being three orders of magnitude greater than the shear modulus. However, since the early 20th century, substantial volume changes have been recorded in reinforced rubbers when first stretched (see for instance [1]). These volume changes are attributed to debonding at the rubber-filler interface and to vacuole formation in the rubber matrix [1,2].

Despite these early volume change observations, it became a standard practice to measure the longitudinal strain and to assume incompressibility in order to reach the stress-stretch response of rubbers submitted to uniaxial tensile tests. Such an assumption renders impossible the study of possible damage and biases the estimation of the actual true stress-stretch response. Later, the measurement of strains has been improved by monitoring them in the longitudinal and transverse directions on one face of the sample. This may be achieved by video extensometry [3,4] or by digital image correlation [5]. Using such techniques coupled to the transverse isotropy assumption, authors reported substantial reversible volume changes [5] in disagreement with the earlier accurate dilatometry measurements [1,6-8] evidencing negligible volume changes for unfilled rubbers and substantial volume changes for filled rubbers during the first load only. However, uniaxial tensile test specimens are usually cut from calendered sheets. Diani et al. [9] observed in-plane anisotropy in such specimens, suggesting an even stronger anisotropy in the thickness direction. Such anisotropy is a plausible explanation for these conflicting results.

The aim of this study is to investigate the strain field along the three spatial directions for a filled elastomer under cyclic uniaxial tension, and in particular analyse volume changes. The measurement of the principal components of the strain tensor provides the true stress-stretch responses and the actual volume changes in samples during cyclic uniaxial tension tests. The latter measurements may lead to a better understanding of the physical mechanisms attached to the Mullins' softening occurring in filled rubbers when first loaded [10].

It is worth emphasising that the proposed methodology has not been proposed in the past to the best of our knowledge, namely, we turn to Digital Image Correlation (DIC) [11] in order to have access to a quantitative estimate of the displacement field and its gradient over regions of interest. Recourse to DIC has already been reported in the past to study elastomers subjected to large strains as discussed below [12,5]. The observation of two free faces with a single camera and an optical prism [13] or two cameras (both viewing the two studied faces and combined with stereo correlation) [14] has been reported. However, side view, optical distortions combined with inhomogeneous strains as encountered in necking leads to limited accuracy in the strain evaluation. In the present study, two independent but synchronized cameras are used to evaluate the mean strain over two orthogonal free faces over a region that is

checked to be homogeneously loaded. This allows for a minimum uncertainty on the measurements. The main difficulty of the proposed approach is to deal with large displacements and their gradients (a classical weak point of DIC) in order to have access to small levels of volumetric strains. A global DIC approach provides us with the required accuracy to detect and measure dilatational strains.

The paper is organized as follow. The next section proposes a brief review on volume variation measurements. Then, material and experimental method are presented in Section 3 and Section 4, respectively. Results are presented in Section 5 and discussed in Section 6. Finally, conclusions close the paper.

2. State of the art

2.1. Mechanical tests

Measurements of volume changes in stretched filled rubbers are carried out using dilatometry or video extensometry. For dilatometry measurements, samples are immersed in a liquid (often water), the volume change of which is measured when the rubber is stretched [15, 1, 6, 7, 8, 16]. Using this technique, Jones and Yiengst [1] measured volume expansions in filled natural rubbers when first stretched. They showed that the volume change is due to vacuoles forming at the rubber-particle interface. On the contrary, unfilled rubbers exhibit very small volume changes, less than 0.2% for 200% stretch, for similar stretching conditions [6]. Mullins and Tobin [7] conducted volume change measurements of previously stretched filled non-crystallizing rubber, and reported relative volume expansion of the order of 10^{-3} upon 400% stretching. Shinomura and Takahashi [8] measured volume change in filled butyl rubber and filled SBR during first loads. They studied the effect of the type of fillers, the filler amount (20, 50 and 70 phr) and the curing. They reported an increase of the volume change with the amount of filler, but more importantly they noticed stretch thresholds of approximately 2.4 and 1.6 below which volume changes were non-measurable for 20 phr and 50 phr filled samples, respectively. The dilatometer measurements are tremendously accurate since relative volume changes as low as 10^{-5} may be detected; nonetheless several minutes are required for each measurement in order to reach the dilatometer equilibrium, making dynamic measurements impossible. Samples may also be placed in a gas chamber connected to a reference chamber by a differential pressure sensor. Chenal et al. [17] used such a Farris apparatus to measure volume changes in stretched filled natural rubber. They measured a 4% volume expansion upon 200%-stretching during cyclic tests. The difficulty with natural rubber is that both cavitation and crystallization contribute with opposite effects on volume change, making any physical interpretation delicate.

Using video extensometry for strain measurement, some authors investigated volume variations measurements of stretched rubber-like materials. Layouni et al. [18] painted seven markers on one face of filled

natural rubber samples and extracted the volume change, assuming the material to be initially isotropic. They reported a reversible change of volume upon cyclic loadings that reached 14% when samples were stretched up to 300%. Le Cam and Toussaint [5] refined the same measurement using DIC. They obtained displacement fields on one face of their samples and assumed transverse isotropy for estimating the volume change of their samples. They conducted tests on 34 phr filled SBR specimens cut into 2 mm thick moulded plates. They reported no significant difference in volume changes between the first cycle, when the material is evidencing substantial Mullins softening, and the consecutive cycles. According to their result, the volume variation (9% for 200%-stretched samples) is linear with respect to the applied stretch and is unrelated to the Mullins softening.

2.2. Other means of study

Elastomers can increase their volume through cavitation which can be seen as an internal phase separation. Such a phenomenon, predictable for energetic reasons [19-21], may occur if the negative pressure decreases below a certain threshold. Experiments with simple liquids [22-24] indicate that in the absence of impurities this threshold is controlled by van der Waals forces. In elastomers however, nucleation occurs on defects and what is observed is cavity growth that is generally occurring when the stress increases beyond the shear modulus. In homogeneous rubbers a certain degree of stress triaxiality is needed for cavity nucleation [25], further leading to their growth at macroscopic scales [26-28].

However, cavities can also form under uniaxial tension when the material is heterogeneous and high triaxiality is present locally. Two situations have been investigated in more details, namely, the cavitation in rubber particles in thermoplastic matrices [29-32] and the cavitation of filled rubbers with large [33,34] or small inclusions [2].

To obtain information on cavity sizes, scattering methods are best adapted to a very large number of small voids. Cavities in filled elastomers have been detected by either light [2] or X-ray [35] scattering methods. In both cases the increase in total scattering signal has been used as a sign of the inception of cavities. In a recent paper, some of the present authors [35] have investigated in detail the scattering from the material investigated in the present study and shown that nanocavities (size 20-50 nm) appear in large numbers when the true stress increases beyond approximately 25 MPa. The purpose of the present paper is to discuss the corresponding macroscopic volume change measurements on the same material.

3. Material

The material used in this study is a cross-linked random copolymer of styrene-butadiene (SBR). The elastomer has a glass transition temperature T_g of −48 °C estimated by DSC. Its density is 0.94 g/cm^3 and the number average molecular mass (M_n) of the starting polymer (before crosslinking) is 120 kg/mol. The mole fraction of styrene is 0.15. A classical crosslinking

system is used based on sulphur and CBS. The crosslinking reaction is activated by zinc oxide (ZnO) and stearic acid. Antioxidant (6PPD) is added. The material contains 60 phr of carbon black (parts of weight per hundred parts of rubber), which corresponds to a volume fraction of 23.9%. The filler is a N347 carbon black with a CTAB (structure parameter) = 87 ± 5 m²/g and DBP (fineness parameter) = 124 ± 5 ml/100g.

The mixing process took place in two steps. The first consisted in mixing elastomer, filler, antioxidant and activators in a chamber at 50 °C. Curing agents (sulphur and CBS) were added on a two-roll mill as a second step. The material composition is summarised in Table 1.

Once mixed, the yet uncured material was calendered and thus transformed into sheets of thickness 2.8 mm (typically 180 mm wide and 1 m long). Next, plates of $150 \times 150 \times 2.8$ mm^3 were punched out of these sheets. They were finally put into a mould of dimensions $150 \times 150 \times 2.5$ mm^3, where they were cured (150 °C for 15 minutes). Because of the contraction of the rubber due to vulcanisation, the mechanical stresses applied during the moulding/curing process remain well below those experienced during calendering. Hence, the latter process is believed to be responsible for a possible anisotropy of these cured plates. Owing to the symmetry of this operation, the material could, therefore, be at most orthotropic, with principal directions of orthotropy along the calendering, transverse and thickness directions.

A few mechanical tests have been conducted to quantify the possible difference of stiffness in the calendaring and transverse directions. Dynamic mechanical analysis applied in simple shear on miscellaneous compounds have shown that, in general, both G' and G" are 5 to 15 % higher in the calendering direction than in the transverse one.

4. Method

4.1. Mechanical test

The uniaxial tensile test consisted of a few load-unload cycles of increasing amplitudes until failure, as shown in Figure 3a. The samples were dumbbell shaped, cut from rubber sheets with a gauge length of 50 mm. The gauge part was 4 mm wide and 2.5 mm thick. The initial distance between clamps was set to 30 mm. With this geometry, the stress state is uniform in the central part of the specimen. It is important to stress that the specimens were not accommodated prior to the test. The material can be considered as being in the as-cast state, devoid of any mechanical alteration other than that due to the cutting operation, which was performed as carefully as possible.

Besides the mechanical testing machine, the setup consisted of two cameras observing, respectively, the front and side face of the sample in order to characterise the strain state of the specimen in three dimensions. To reduce the effect of the out of plane displacements on the measured displacement field [36], quasi-telecentric lenses were used for both cameras. Figure 1 shows the experimental setup. The front camera acquired 4096×1400 pixel images while the side face one was limited to 800×1040 pixels. The physical size of

one pixel corresponds to 3.7 and 6.9 µm, respectively, for the face and side images. A total of 1185 images were recorded from each camera. However, essentially because of the large displacements incurred by the specimen, and the required synchronization, not all pictures could be exploited. A little more than 700 image pairs could be reliably exploited to follow the experiment.

Because of the large strains considered in this study, it was not possible to keep the cameras fixed during the test as the studied domain would be progressively moved out of the field of view. Therefore, the cameras were mounted on micrometric elevation stages shown in Figure 1. The repositioning of the camera was, however, limited to a minimum number of moves. Markers present on both observed faces allowed for a crude adjustment of the field of view. The detailed DIC analysis will provide the required translation information to account for this change in the analysis. Moreover, images were taken before and after the camera repositioning at fixed displacement of the sample to check that no spurious artefactual strain would result from such steps.

4.2. DIC principle

Digital Image Correlation is a technique that consists in registering images acquired at different stages of loading in order to retrieve the displacement field experienced by the sample [11]. The sensitivity of the method relies primarily on a well contrasted pattern present on the observation surface. Because the SBR specimen is very homogeneous, a speckle pattern has to be deposited on the surface. This marking should not interfere with the behaviour of the material, and has to withstand very large strains without debonding from the surface. The cleaned surface was sprayed with a fine white talc powder. Surface Van der Vaals forces proved sufficient to make those particles stay adhered for the duration of the test. Figure 2 shows the observed surfaces and their speckle.

Different DIC strategies have been used to provide a measurement of the displacement field. The most common one, termed “local” and used by most commercial DIC codes, is based on the partitioning of the image into small zones, each of which being characterized by the mean translation of its centre. The DIC code in the present study is based on a different – “global” – approach, where the displacement field is decomposed over a chosen basis, the amplitudes of which are determined globally over the entire region of interest. Such an approach has been shown to be suited to follow large strains as encountered for polymeric materials [12]. A convenient basis uses finite-element shape functions defined over a regular mesh supported by the pixel structure of the images. A uniform square grid is utilised in the sequel, with quadrangular bi-linear elements. The advantage of this technique is to impose a continuity of the displacement field, which turns out to reduce the uncertainty of the analysis. The reader is referred to Ref. [37] for details of the DIC algorithm.

The specific difficulty of using DIC for elastomeric materials is the large amplitude of displacements that may prevent a proper determination of the displacement [38-40]. To overcome this difficulty, images were acquired at

small loading increment (typically for an incremental axial strain of order 2-3 %) and the displacement analysis was partitioned into subseries (the displacement field was computed from time t_i to time t_j, for $t_j - t_i < 50$ images). The subseries could then be combined to obtain the absolute displacement from the reference image. However, for the present purpose, this operation is unnecessary as one is essentially interested in the transformation gradient, which can be combined directly, once they have been evaluated from the incremental displacement fields. The full displacement fields are thus used as an intermediate step in order to validate the fact that a homogeneous strain is a good representation of the actual strain. The cumulative effect of uncertainties is present, yet its level is low enough not to be limiting.

4.3. DIC Analysis

The kinematics of the test was expected to be simple (uniform strain over the studied domain), hence large element sizes (64×64 pixels) could be used leading to a small uncertainty. Although a single element would have been sufficient to capture a uniform strain, the region of interest was partitioned into a few elements to validate the strain homogeneity.

The first step of the analysis consisted in estimating the a priori uncertainty of the displacement and strain evaluation. The latter depend on the speckle pattern and chosen mesh size. For the two image series, the displacement uncertainty due to DIC was measured to be 10^{-3} pixel, and the strain uncertainty was 10^{-5}. Additional features, such as the change of the surface texture and acquisition noise, lead to higher values of the uncertainty

From the measured (Lagrangian) displacement field, the mean gradient is obtained from a linear regression

$$U_i = A_i + G_{ij}\, x_j$$

so that the deformation gradient tensor $\boldsymbol{F}$ is equal to $\boldsymbol{I} + \boldsymbol{G}$. If the length (resp. width and thickness) axis is labelled 1 (resp. 2 and 3), the face camera gives access to F_{11}, F_{12}, F_{21} and F_{22}, whereas the side camera provides F_{11}, F_{13}, F_{31} and F_{33}. Only the shear component and rotation around the tension axis F_{23} and F_{32} cannot be estimated from these observations. However, both of these components are expected to be null and, moreover, their contribution to det($\boldsymbol{F}$) is low. It is also to be noted that the axial strain F_{11} is determined independently from both sets of images. Thus the comparison between these two evaluations constitutes a partial validation of the analysis.

From the determination of the deformation gradient, one can evaluate the volumetric strain

$$\varepsilon_V \equiv \frac{\Delta V}{V_0} = \det(\boldsymbol{F}) - 1$$

Principal stretches are obtained (taking square roots) from the eigenvalues of the right Cauchy Green deformation tensor $\boldsymbol{C} = \boldsymbol{F}\,{}^t\boldsymbol{F}$. The three eigenvalues are observed to always coincide with the principal axes of the sample.

It is noteworthy that the actual elongation measurement differs slightly from the nominal value estimated by the prescribed displacement divided by

the specimen length. This effect is due to the dumbbell shape of the specimen and slip in the grips.

5. Results

Figure 4a shows the two minor principal stretches, λ_2 and λ_3, as functions of λ_1. Each of them seems to follow an almost reversible change since, throughout all cycles, the data collapses onto a single curve. However, there are small yet significant deviations from this trend. The second salient feature that appears in this figure is the fact that, although the test is uniaxial tension, the two transverse stretches are clearly different, from the smallest to the largest elongations. When plotted against each other, as shown in Figure 4b, a linear relationship is found to fit the data very well over the entire range covered by the experiment. The latter is written as

$$1 - \lambda_2 = \alpha(1 - \lambda_3)$$

A linear regression leads to the following estimate of the parameter, $\alpha = 0.90$. Since the sample was virgin (undeformed) prior to the mechanical test, this anisotropic behaviour is probably due to calendering. Note however that the present anisotropy cannot be directly compared with that previously mentioned (obtained in dynamic mode, with much lower amplitudes, in simple shear, and comparing directions 1 and 2).

Although Figure 4a shows a quasi-reversible behaviour, slight departures are seen for large elongations. This results from a breakdown of incompressibility. To highlight this phenomenon, let us consider the volume, given by $\det(\boldsymbol{F})$ (or equivalently $\lambda_1\lambda_2\lambda_3$), whose evolution with the principal elongation is shown in Figure 5. On this plot, the entire history of cycling is shown. For the first cycles, the volume remains invariant, i.e. the behaviour can be considered as incompressible. The fluctuations, less than 1%, correspond to the actual uncertainty of the measurement, which in addition to the pure DIC uncertainty cumulates the errors due to the entire experimental chain of data acquisition. These fluctuations are more apparent in this plot than in Fig. 4 because of the fact that the reference is flat. However, past a stretch level of about $\lambda_1 \approx 2.5$, the specimen expands well above the uncertainty level. Upon unloading, a hysteretic behaviour is observed, but the sample recovers its original volume for an elongation of about 2.3, and remains incompressible for lower values. An unexpected feature appears in the next load cycle: Now, no volume changes are observed for elongations less than the maximum value reached in the previous cycle. Then, as soon as this elongation is reached, a volume expansion takes over abruptly. For this cycle again, unloading is hysteretic with a more pronounced difference on the return path. The next (and final loading stage) shows very clearly the very same behaviour as observed for the previous cycle, namely, the volume remains approximately constant up to the maximum elongation experienced in the past, and suddenly increases past this value. Unfortunately, failure of the sample before the maximum load aimed at interrupted the test.

6. Interpretation and Discussion

6.1. Additional information

The same material was subjected to uniaxial and monotonic loading until fracture and probed by synchrotron X-ray radiation [35]. Cavities appeared above a similar stretch threshold ($\lambda_1 \approx 2.5$), indicated by the development of a streak perpendicular to the tensile axis in the reciprocal space. The related scattering invariant that is proportional to the total amount of scatterers inside the system abruptly increases in the same manner. A more complete analysis of the 2D scattering patterns shows the shape of the voids are close to lozenge or ellipsoid and elongated in the tensile direction. Their average size lies within 20-40 nm. Cavities created far beyond the stretch threshold are smaller in size but maintain a constant aspect ratio (major to minor axis of 1.6). The volume fraction of these nanovoids can be calculated from the measured scattering patterns by a three-phase model and the result is comparable with that from digital image correlations. Upon cyclic testing the variations of the scattering invariant with strain closely parallel the changes in macroscopic volume observed here, and the detailed analysis of the X-ray data will be the object of a forthcoming paper.

6.2. Discussion

It is to be noted that the results presented here are the first obtained by a DIC analysis that reproduces the volume changes measured by dilatometry reported in the literature. These results confirmed that, for a highly filled rubber submitted to uniaxial stretch:

- its volume expands when the rubber is stretched above a threshold, here approximately, $\lambda_1 \approx 2.5$.
- its volume expands when the rubber is stretched beyond the maximum stretch ever applied,
- its volume remains quasi constant when the rubber is stretched below the maximum stretch ever applied

The difference between λ_2 and λ_3 reported in Figure 4a shows the non-transverse isotropy of the material. The transverse stretch λ_2 appears to be always greater than $\lambda_1^{-1/2}$. A volume estimate with λ_1 and λ_2 only, assuming transverse anisotropy as proposed in [5], leads to an erroneous quasi reversible positive volume change during cyclic loadings.

In terms of filled rubbers stress-stretch responses, the usually admitted incompressibility assumption introduces an overestimate of the Cauchy stress. Nonetheless, this difference only becomes noticeable at high stretch, typically $\lambda_1 = 4$ for the present material. The threshold elongation for volume expansion increases when decreasing the amount of fillers [8], incompressibility holds for low filler content and low stretch. Moreover, past the first loading, the volume remains constant in uniaxial extension. Finally, the measurements revealed an initial anisotropy of the plates, while initial isotropy is generally assumed. This may have an impact on complex models revealing the anisotropy induced by the Mullins softening.

7. Conclusions and perspectives

A cyclic uniaxial tension experiment on a carbon-black filled SBR sample was studied. Digital image correlation was used to follow the kinematics of two orthogonal free faces. This technique showed its ability to deliver a precise measurement of the transverse and longitudinal strains, and the corresponding estimation of the relative volume variation. Starting from a virgin material, the volume evolution can thus be followed as a function of the full longitudinal extension history of the region of interest.

During the first stretching, no significant variations of the volume of quasi incompressible elastomers were detected up to a reproducible level of extension. A monotonic volume expansion was then observed past this critical extension, which can be interpreted as the onset of cavitation.

Under cyclic loading, the full deformation history plays an important role. At first unloading, the volume increase observed during initial stretching progressively decreases and then completely disappears. However, unexpectedly, during the following cycles, volume expansion remains close to zero until the maximal elongation previously reached. Past this value an abrupt volume expansion is observed. This behaviour is reminiscent of Mullins softening, in the sense that the first experience of a load level produces significant "damage", whereas further cycles below the maximum stress shows more reversible behaviour. Similarly, filler, known to be responsible for Mullins softening, appears necessary to generate local confined regions where local stress enhancement and triaxiality allow for the nucleation of cavities. However, it is to be stressed that the Mullins effect is observed for elongations well below those necessary to trigger a volume change. Therefore, one cannot draw a direct link between volume expansion and the Mullins effect.

All the results presented here confirm prior SAXS investigations performed on identical samples undergoing exactly the same conditioning, which reveal the nature of the volume change, i.e. the nucleation and growth of nanovoids (20-50 nm in size) [35]. In the latter study, volume variations are not directly measured but are interpreted from a quantitative modelling of the scattered intensity from nanovoids. The expansion estimates are quite comparable although these techniques are based on extremely different length scales (macroscopic for DIC, and nanometric for SAXS). Slight discrepancies may be expected inasmuch as the SAXS detection window is limited and cannot appreciate large cavities beyond the window, yet the agreement is quite remarkable. In particular, the onset of cavitation coincides precisely in both measurements, and the irreversible closing of cavities after unloading is indeed observed in both experiments.

To enhance the understanding of the link between cavitation, stress softening, and permanent set, it is important to combine macroscopic tests with more local measurements of damage mechanisms.

Acknowledgements

The present work is supported by the French Agence Nationale de la Recherche (ANR) through the AMUFISE project (MATETPRO 08_320101).

References

1. Jones H.C., Yiengst H.A., 1941. Dilatometer Studies of Pigment-Rubber Systems, Rubber Chem. Technol. **14**, 113-124.

2. Ramier J., Chazeau L., Gauthier C., Stelandre L., Guy L., Peuvrel-Disdier E. (2007). In situ SALS and volume variation measurements during deformation of treated silica filled SBR. Journal of Materials Science **42**(19): 8130-8138.

3. G'Sell C., Hiver J.-M., Dahnoun A., Souahi A. (1992) Video-Controlled Tensile Testing of Polymers and Metals Beyond the Necking Point. J. Mat. Sci., **27**, 5031-5039.

4. Wu, J.D. and Liechti, K. M., 2000. Multiaxial And Time-Dependent Behavior Of A Filled Rubber, J. Time-Dependent Mater. 4, 293-331

5. Le Cam J.B., Toussaint E., 2009. Cyclic volume changes in rubber, Mech. Mater. **41**, 898-901.

6. Gee G., Stern J., Treloar L.R.G., 1950. Volume changes in the stretching rubber, Trans. Faraday. Soc. **46**, 1101-1106.

7. Mullins L., Tobin N.R., 1958. Carbon-black loaded rubber vulcanizates: Volume changes in stretching, Rubber Chem. Technol. **31**, 505-512

8. Shinomura T., Takahashi M., 1970. Volume change measurements of filled rubber vulcanizates under stretching, Rubber Chem. Technol. **43**, 1025-1035.

9. Diani J., Brieu M., Vacherand J.M., Rezgui A., 2004. Directional model for isotropic and anisotropic hyperelastic rubber-like materials, Mech. Materials 36 (4) 313-321

10. Mullins L., 1969. Softening of rubber by deformation, Rubber Chem. Technol. **42**, 339-362.

11. Sutton M.A., Orteu J.-J., Schreier H. (2009) Image correlation for shape, motion and deformation measurements: Basic Concepts, Theory and Applications. Springer.

12. Chevalier L., Calloch S., Hild F., Marco Y. (2001). Digital image correlation used to analyze the multiaxial behavior of rubber-like materials, Eur. J. Mech. A/Solids **20,** 169–187

13. Parsons E., Boyce M.C., Parks D.M., 2004. An experimental investigation of the large-strain tensile behavior of neat and rubber-toughened polycarbonate, polymer, **45**, 2665-2684.

14. Grytten F., Daiyan H., Polanco-Loria M., Dumoulin S., 2009, Use of digital image correlation to measure large-strain tensile properties of ductile thermoplastics, Polymer Testing **28**, 653-660

15. Holt W.L., McPherson A.T., 1936. Change of volume of rubber on stretching: Effects of time, elongation and temperature, J. Res. Natl. Bur. Stand. **17**, 657-678.

16. Kumar P., Thomas A.G., Fukahori Y., Busfield J.J.C., 2007. Cavitation in granulate filled rubber materials. Proceedings of the 5th European Conference on Constitutive Models for Rubber, ECCMR 2007, 157-163.

17. Chenal J.M., Gauthier C., Chazeau L., Guy L., Bomal Y., 2007. Parameters governing strain induced crystallization in filled natural rubber, Polymer **48**, 6893.

18. Layouni K., Laiarinandrasana L., Piques R., 2003. Compressibility induced by damage in carbon black reinforced natural rubber. Proceedings of the 3rd European Conference on Constitutive Models for Rubber, ECCMR 2003 , 273-281.

19. Ball J.M. (1982). Discontinuous Equilibrium Solutions and Cavitation in Non-Linear Elasticity. Philosophical Transactions of the Royal Society of London, series A: Mathematical, Physical and Engineering Sciences **306**: 557-611.

20. Horgan C.O., Polignone D.A. (1995). Cavitation in nonlinearly elastic solids: A review. Appl Mech Rev **48**(8): 471-485.

21. Dollhofer J., Chiche A., Muralidharan V., Creton C., Hui C.Y. (2004). Surface energy effects for cavity growth and nucleation in an incompressible neo-Hookean material - modeling and experiment. International Journal of Solids and Structures **41**(22-23): 6111-6127.

22. Fischer J.C. (1948). The fracture of liquids. Journal of Applied Physics **19**: 1062-1067.

23. Briggs, L.J. (1950). Limiting negative pressure of water. Journal of Applied Physics **21**: 721-722.

24. Briggs, L.J. (1951). The limiting negative pressure of acetic acid, benzene, aniline, carbon tetrachloride, and chloroform. Journal of Chemical Physics **19**(7): 970-972.

25. Hou H.S., Abeyaratne R. (1992). Cavitation in Elastic and Elastic Plastic Solids. Journal of the Mechanics and Physics of Solids **40**(3): 571-592.

26. Gent A.N., Lindley P. B. (1959). Internal rupture of bonded rubber cylinders in tension. Proceedings of the Royal Society of London, series A: Mathematical and Physical Sciences **249** A: 195-205.

27. Denecour R.L., Gent A.N. (1968). Bubble formation in vulcanized rubbers. Journal of Polymer Science, Part A-2 Polymer Physics **6**: 1853-1861.

28. Cristiano A., Marcellan A., Long R., Hui C.Y., Stolk J., Creton C. (2010). An experimental investigation of fracture by cavitation of model elastomeric networks. Journal of Polymer Science Part B: Polymer Physics **48**(13): 1409-1422.

29. Bucknall, C. B., Karpodinis A., Zhang X.C. (1994). A Model for Particle Cavitation in Rubber-Toughened Plastics. Journal of Materials Science **29** (13): 3377-3383.

30. Magalhães A.M.L., Borggreve R.J.M. (1995). Contribution of the crazing process to the toughness of rubber-modified polystyrene. Macromolecules **28**: 5841-5851.

31. Fond C., Lobbrecht A., Schirrer R. (1996). Polymers toughened with rubber microspheres: An analytical solution for stresses and strains in the rubber particles at equilibrium and rupture. International Journal of Fracture **77**(2): 141-159.

32. Ayre D.S., Bucknall C.B. (1998). Particle cavitation in rubber-toughened PMMA: experimental testing of the energy-balance criterion. Polymer **39** (20): 4785-4791.

33. Gent A.N., Park B. (1984). Failure processes in elastomers at or near a spherical inclusion. Journal of Materials Science **19**: 1947-1956.

34. Cho K., Gent A.N., Lam P.S. (1987). Internal fracture in an elastomer containing a rigid inclusion. Journal of Materials Science **22**: 2899-2905.

35. Zhang, H., Scholz A.K., de Crevoisier J., Vion-Loisel F., Besnard G., Hexemer A., Brown H.R., Kramer E.J., Creton C. (2011). Nanocavitation in Carbon Black Filled Styrene-Butadiene Rubber under Tension Detected by Real Time Small Angle X-ray Scattering. Submitted to Macromolecules.

36. Sutton M.A., Yan J.H., Tiwari V., Schreier H.W., Orteu J.-J. (2008). The Effect of Out of Plane Motion on 2D and 3D Digital Image Correlation Measurements. Optics Lasers Eng., **46**, 746-757.

37. Besnard G., Hild F., Roux S. (2006). Finite-element displacement fields analysis from digital images: Application to Portevin-Le Châtelier bands, Experimental Mechanics **46**, 789-803

38. Elnasri I., Pattofatto S., Zhao H., Tsitsiris H., Hild F., Girard Y. (2007). Shock enhancement of cellular structures under impact loading: Part I Experiments. J. Mech. Phys. Solids, **55**, pp. 2652-2671.

39. Tarigopula V., Hopperstad O.S., Langseth M., Clausen A.H., Hild F., Lademo O.-G., Eriksson M. (2008). A Study of Large Plastic Deformations in Dual Phase Steel Using Digital Image Correlation and FE Analysis. Exp. Mech., **48**, 181-196.

40. Besnard G., Lagrange J.-M., Hild F., Roux S., Voltz C. (2010). Characterization of necking phenomena in high speed experiments by using a single camera, EURASIP J. Im. Video. Proc., 2010 (215956), 1-15

Figure Captions

Figure 1: Schematic plot of the experimental set-up. Two cameras take pictures of two orthogonal free faces of the sample subjected to uniaxial tension.

Figure 2: Front (a) and side (b) images of the specimen. The surface texture is obtained from a talc powder dispersed onto the surface of the SBR sample. This patterning is necessary for Digital Image Correlation.

Figure 3: (a) Loading history of the sample nominal elongation (relative displacement scaled by the sample length) versus time, *t*. (b) Tensile force versus nominal elongation.

Figure 4: (a) Minor principal stretches λ_2 and λ_3 versus elongation λ_1 (major stretch). The dotted curve indicates the expected behaviour for an isotropic incompressible material, ($\lambda_t = 1/\sqrt{\lambda_1}$). (b) Stretch along the width versus that along the thickness is shown for all cycles as a bold curve. The dotted line is a linear regression through the data with a slope of 0.90.

Figure 5: Relative volume versus elongation. Arrows indicate the temporal ordering. Note that in the reloading stage of each cycle, there is no significant volume variation until λ_1 reaches the maximum stretch experienced in the past. Expansion, whose onset is evaluated to $\lambda_1 \approx 2.5$, is interpreted as due to cavitation of nanovoids.

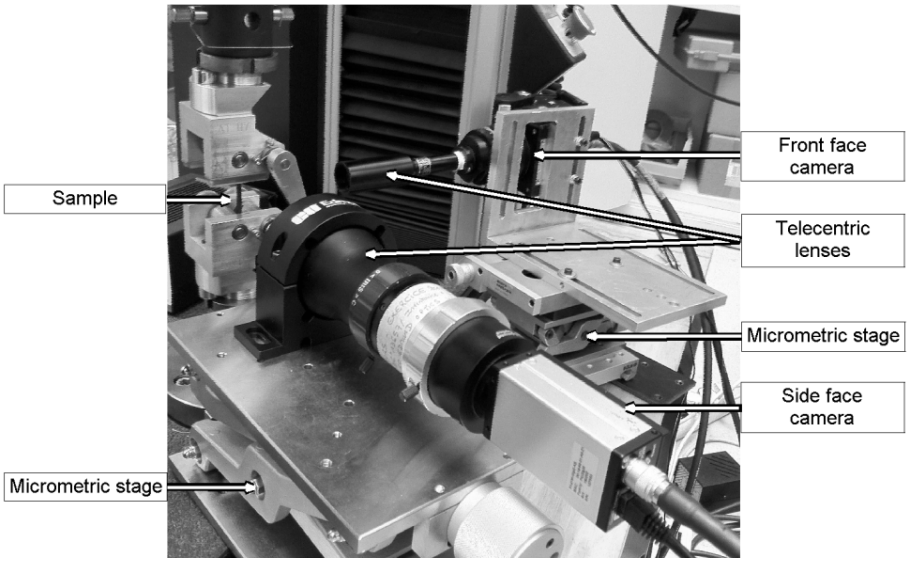
Front face camera
Sample
Telecentric lenses
Micrometric stage
Side face camera
Micrometric stage

Figure 1

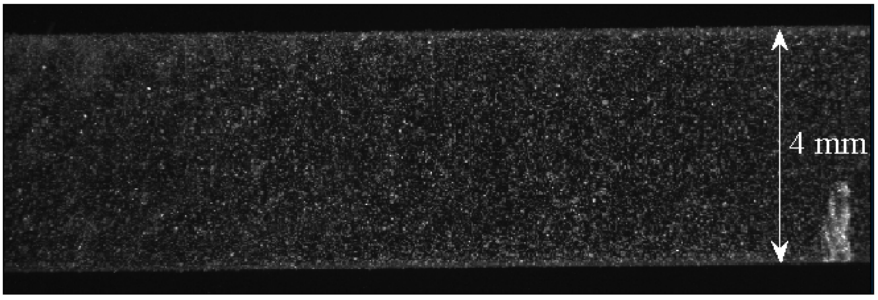

(a)

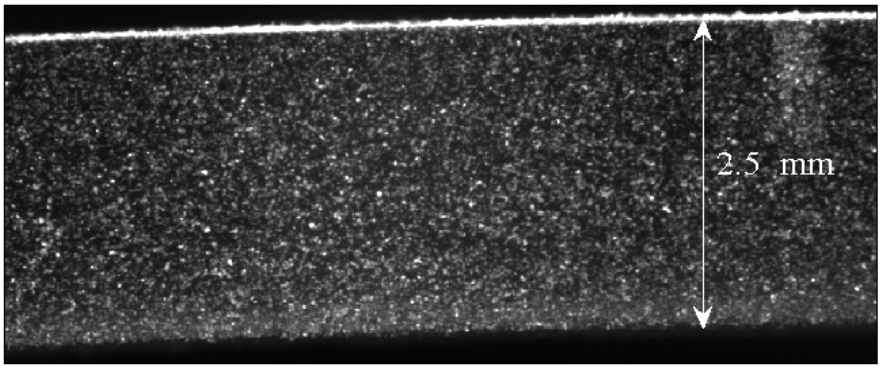

(b)

Figure 2

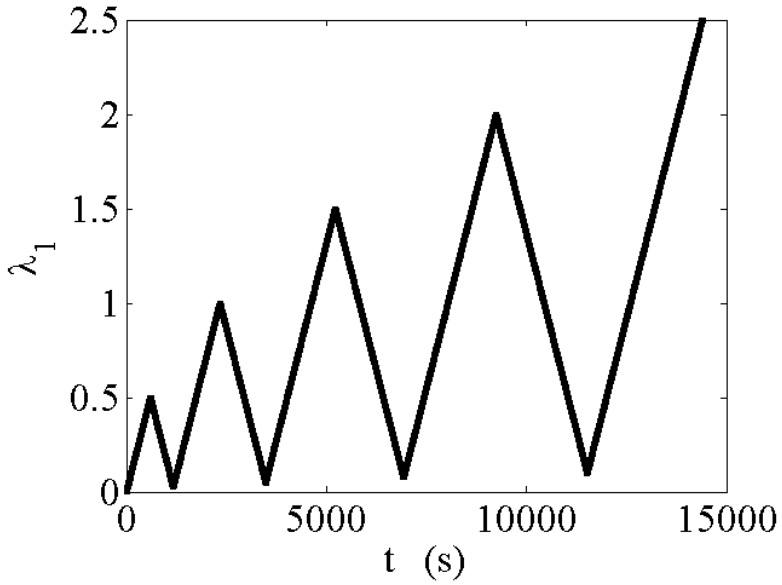
2.5
2
1.5
1
0.5
0
λ_1
0
5000
10000
15000
t (s)

(a)

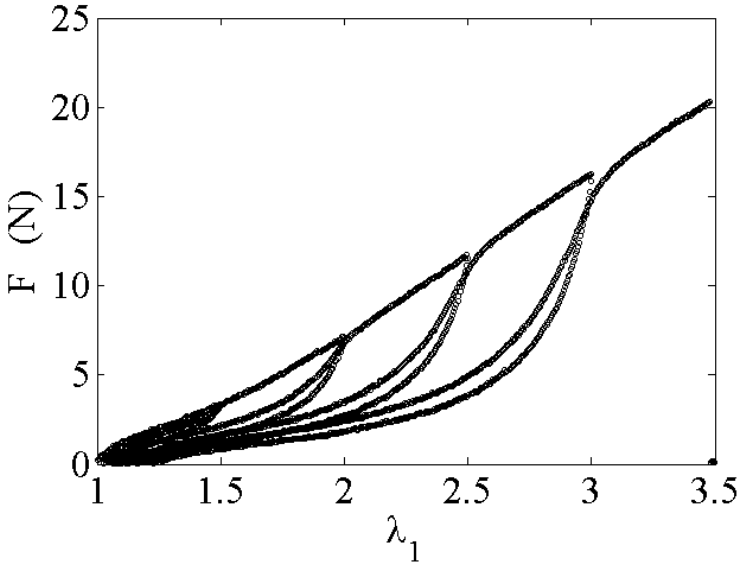
25
20
15
10
5
0
F (N)
1
1.5
2
2.5
3
3.5
λ_1

(b)

Figure 3

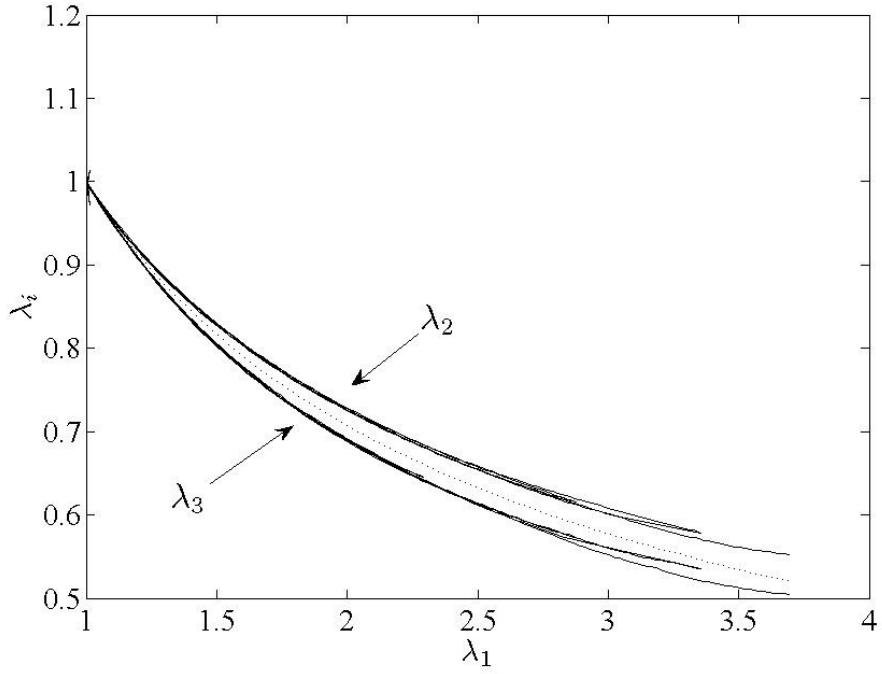
1.2
1.1
1
0.9
0.8
0.7
0.6
0.5
λ_i
λ_2
λ_3
1
1.5
2
2.5
3
3.5
4
λ_1

(a)

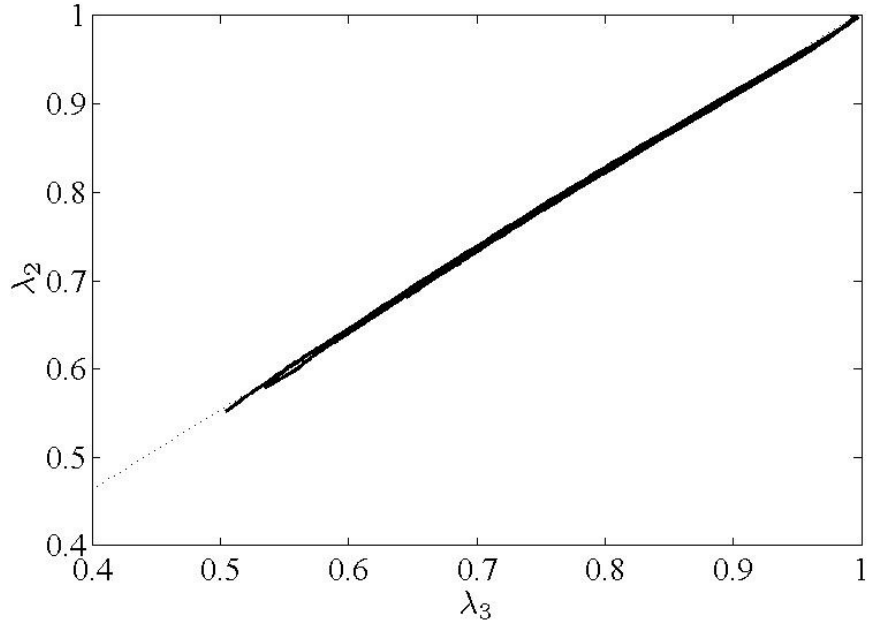
1
0.9
0.8
0.7
0.6
0.5
0.4
λ_2
0.4
0.5
0.6
0.7
0.8
0.9
1
λ_3

(b)

Figure 4

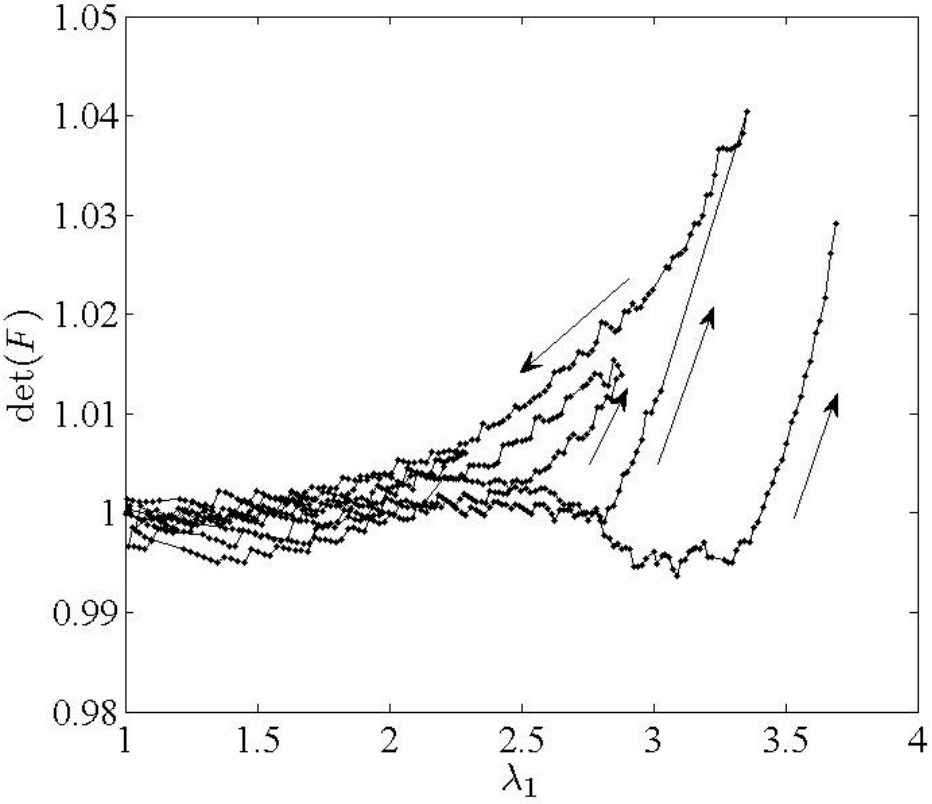

Figure 5